MIXED MATRIX MEMBRANES COMPRISING MOFS AND POROUS SILICATE FILLERS PREPARED VIA SPIN COATING FOR GAS SEPARATION

Philipp Burmann[a], Beatriz Zornoza[b]*, Carlos Téllez[b], Joaquín Coronas[b]

[a]Technische Universität München, Department of Chemistry, Lehrstuhl 1 für Technische Chemie, 85747 Garching, Germany

[b]Chemical Engineering Department and Nanoscience Institute of Aragon, Universidad de Zaragoza, 50018 Zaragoza, Spain

* Corresponding author:

Dr. Beatriz Zornoza Encabo

Chemical Engineering Department and Nanoscience Institute of Aragon

Universidad de Zaragoza

C/ Mariano Esquillor s/n. 50018 Zaragoza. Spain

Phone: 34 876 555427. Fax: 34 976 761879

e-mail: bzornoza@unizar.es

ABSTRACT

Different types of fillers of inorganic (titanosilicate ETS-10 and mesoporous silica type MCM-41) and organic-inorganic nature (ZIF-8 and NH_2-MIL-53), with different pore size (micro- and mesoporosity) and structure, diverse particle shape, and particle sizes in the 85-400 nm range were embedded in a polysulfone matrix via spin coating. Spin coating technology, widely used in the production of thin and uniform layers on porous was used here to fabricate in one coating step symmetric mixed matrix membranes (MMMs) by adjusting the spinning disk velocity, rotational time, and solid concentration and volume of solution. By selecting the optimal parameters, homogeneous MMMs containing 8 wt.% of the various fillers were tested for H_2/CH_4 and O_2/N_2 mixed-gas separations, obtaining significant improvements over the neat polymer. While NH_2-MIL-53 MMMs revealed the highest separation performance (a rise in selectivity of 50-60% compared to the pure polymer for both H_2/CH_4, and O_2/N_2 separations), ZIF-8 MMMs showed a substantial increase in permeability (from 12.7 to 51.4 Barrer for H_2/CH_4, and from 2.0 to 6.5 Barrer for O_2/N_2). Besides, the spin coating process enhanced solvent evaporation and reduced coat production time compared to the traditional by-hand casting.

***Keywords*:** Mixed-matrix membrane; Spin coating; Mixed-gas separation; Polysulfone; Metal-organic framework; Mesoporous silica; Titanosilicate.

1. INTRODUCTION

One of the most significant challenges in the development of membrane technology for gas separation processes is the fabrication of so-called mixed matrix membranes (MMMs) as an alternative to neat polymers with the aim of improving the overall membrane effectiveness. With MMMs, the superior gas separation properties of the embedded porous sieves used as fillers are combined with the economical processability and desirable mechanical properties of continuous polymer matrices (Kulprathipanja et al., 1988). Research into these hybrid films has attracted the attention of the membrane community during the past two decades, and hundreds of articles have been published on the subject including several reviews (Aroon et al., 2010; Bernardo et al., 2009; Chung et al., 2007; Goh et al., 2011). Among the different families of fillers, zeolites (Moore et al., 2004; Zimmerman et al., 1997; Zornoza et al., 2011b), porous titanosilicates (Rubio et al., 2010), ordered mesoporous silica (Reid et al., 2001; Zornoza et al., 2011a), non-porous silica (Ahn et al., 2008; Merkel et al., 2002), carbon molecular sieves (CMSs) (Vu et al., 2003), or carbon nanotubes (Kim et al., 2007), among others, have been incorporated into polymers to produce MMMs, seeking to overpass the Robeson upper-bound (Robeson, 1991; Robeson, 2008). Lately, the research trend in MMMs has shifted towards the utilization of metal-organic-frameworks (MOFs) (Bae et al., 2010). The combination of organic and inorganic building blocks in MOFs offers an almost infinite number of structures, a high degree of flexibility in pore size and shape, and considerable functionalization potential.

Academic community has been actively working on fabricating flat dense MMMs for gas separation. Generally, these membranes include a thick dense selective layer with consequent lower gas permeation flux (Li et al., 2006). To further expand the applications of MMMs for industrial implementation, a more effective membrane type,

asymmetric hollow fiber membranes, is being explored (Husain and Koros, 2007; Rafizah and Ismail, 2008). These have a larger membrane area per volume, good flexibility and easy processing in the fabrication of the module. Reducing the layer thickness is one of the most important challenges for the successful performance of membranes due to the need for high rates of gas production (Jiang et al., 2006; Tanh Jeazet et al., 2012).

At the laboratory scale, MMMs are typically prepared with a casting solution comprising the dispersed filler and the continuous polymer matrix, where the dense membrane is formed when evaporating the solvent in a controlled environment. Traditionally, the casting is made on flat glass by hand, either in a Petri dish or a doctor blade system. This work explores a semi-automatic method of producing homogeneous MMMs by means of spin coating technology.

Spin coating is normally used for the deposition of thin films on disks for the protection of metals, plastic, or electrical circuits. Also, integrated optics or hosts for biochemical processes can be produced with these types of coatings (Zhang et al., 2004). One of the most well-known applications is the coating of circular semiconducting silicon slices up to 300 mm in diameter. In this application, various layers of coats that are processed by microlithography are applied to form integrated circuits for computer processors (Oztekin et al., 1995). This technology has also been used to prepare thin membranes where the support is typically part of the final asymmetric membrane and the coated layer is very thin due to the spill out of the precursor solution over the edge of the support. Asymmetric carbon molecular sieve membranes (CMSs) from the pyrolysis of a polyetherimide (Itta et al., 2010) or a poly(phenylene oxide) (PPO) layer (Itta et al., 2011) coated on a macroporous alumina disk as support were prepared using spinning velocities of 2,000 rpm with a resulting

dense carbon layer about 3 μm thick. Also coated over alumina substrate, Rao et al., 2008 and Tseng et al., 2009 incorporated multi-wall carbon nanotubes into polyetherimide and polyimide precursor solutions, respectively, increasing membrane permeability and selectivity; and Weng et al., 2010 prepared multi-layer membranes with a PPO/SBA-15 silica sieve on a CMS/Al_2O_3 substrate. Poly (4-methyl-1-pentene) (PMP) selective layer of 25-75 μm was also casted onto a microporous PSF substrate via spin coating (Leroux and Paul, 1992). In addition, thin polyimide layer membranes on silica wafers, 200 nm in thickness, and subsequently coated with a 3 μm thick polydimethylsiloxane (PDMS) layer were prepared by Cui et al., 2011; and Shen and Lua, 2010 fabricated polyimide membranes with thicknesses ranging from 6 to 310 μm on dense poly(methyl methacrylate) (PMMA) substrates.

However, the preparation of symmetric MMMs via spin coating, where only a temporary support is used, has scarcely been explored. This method represents a fast and viable form of homogeneous symmetric lab-scale membrane preparation. The main focus of this research is the production of MMMs comprising MOFs and porous silicate fillers using the spin coating technology. First, a processability study of producing membranes via spin coating was carried out, analyzing the influence of the rotational speed, precursor volume, solid concentration and rotation time. Secondly, MMMs based on polysulfone (PSF) were fabricated with different types of fillers varying in nature, size, shape and porosity: (*i*) titanosilicate ETS-10, (*ii*) mesoporous silica MCM-41, and MOFs (*iii*) ZIF-8 and (*iv*) NH_2-MIL-53. The membranes obtained were evaluated for their performance in the separation of H_2/CH_4 and O_2/N_2 binary mixtures.

2. EXPERIMENTAL

2.1. Materials and synthesis

Four different types of fillers were used for the preparation of MMMs. For the synthesis of the titanosilicate ETS-10, sodium metasilicate solution (25.5-28.5% SiO_2, 7.5-8.5% Na_2O, Merck), potassium chloride (p.a., Panreac), potassium fluoride (99%, Sigma Aldrich), titanium(IV) oxide anatase powder (TiO_2, 99.8%, Sigma Aldrich; particle size range 100-300 nm) and distilled water were used, following a procedure described by Casado et al., 2009. The MCM-41 type mesoporous silica spheres were prepared as described by Grün et al., 1997 by using cetyltrimethylammonium bromide (CTABr, >98%, Sigma–Aldrich), tetraethoxysilane (TEOS, 98%, Sigma Aldrich), ammonia (NH_4OH, 25%, Panreac), ethanol absolute (Panreac) and distilled water. Zeolite imidazolate framework (ZIF) ZIF-8 was produced following the synthesis route developed by Pan et al., 2011 with the reactants zinc nitrate hexahydrate ($ZnNO_3 \cdot 6H_2O$, >98%, Sigma-Aldrich), 2-methylimidazole ($C_4H_6N_2$, >99%, Sigma-Aldrich) and distilled water. NH_2-MIL-53, was obtained following the synthesis procedure described by Couck et al., 2009 using aluminum nitrate nonahydrate ($Al(NO_3)_3 \cdot 9H_2O$, 98%, Sigma-Aldrich), 2-amino-terephthalic acid (99%, Sigma-Aldrich) and N,N-dimethylformamide (DMF, >99%, Sigma-Aldrich).

Polysulfone Udel® P-3500 (PSF) was kindly supplied by Solvay Advanced Polymers and chloroform (>99%) was purchased from Sigma-Aldrich.

2.2. Membrane fabrication

2.2.1. Preparation of the precursor solution

MMMs were prepared containing 8 wt.% filler concentration (filler/(filler + polymer)), being the loading that gave an optimal permeability-selectivity binomial for mesoporous silica based MMMs in previous works (Zornoza et al., 2011a; Zornoza et al., 2009). Each type of filler, separately, was dispersed in the solvent (chloroform) in an ultrasound bath during 30 min. Then polysulfone pellets were added in three separate

fractions (1/6, 2/6 and 3/6) while stirring at intervals of a minimum of 2 h each, obtaining a final solid concentration of 12.5-15 wt.% in the dispersion ((filler + polymer) / (filler + polymer + solvent)). After each polymer addition step, the precursor solution was put into an ultrasound bath for 10 min and finally stirred for 24 h. The precursor solution containing 0.52 g of filler, 6.00 g of polymer and 45.65 g of solvent was used for the preparation of about 8-10 membranes. For bare polymer membranes, the solution (12.5-15 wt.% polymer / (polymer + solvent)) was stirred overnight previous to the casting.

2.2.2. Casting by spin coating

A spin coater (Laurell WS-650-23) was used to fabricate feasible tailored membranes in a semi-automatic way. First, the temporary support (Petri dish) was centrally placed onto the rotational chuck, as Fig. 1 schematically shows. Once the spin coater lid was closed, a nitrogen gas purge was applied at 4 bar. An external vacuum pump provided the vacuum that drives the rotational device. The desired parameters of the spinning process were entered in the control panel. A two-step sequence was applied. The first was an acceleration step of 1,000 rpm/s for 5 s until an end-speed of 200 rpm which was kept constant for all membranes. In the second step, the rotational velocity and rotational time, where the membrane formation and evaporation of the solvent mainly took place was studied. The velocity was set in a range of 160-1,000 rpm for stability and security reasons. Simultaneously to the start of the spinning process sequence, the desired amount of precursor solution was sprayed from an injector (a syringe) onto the Petri dish, where it was spread evenly by the centrifugal force. Finally, the cast membrane was left out of the device partially capped to continue the natural evaporation and was subsequently placed in a vacuum oven under a vacuum of 10 mbar and a temperature of 120 ºC for 24 h to complete the solvent removal.

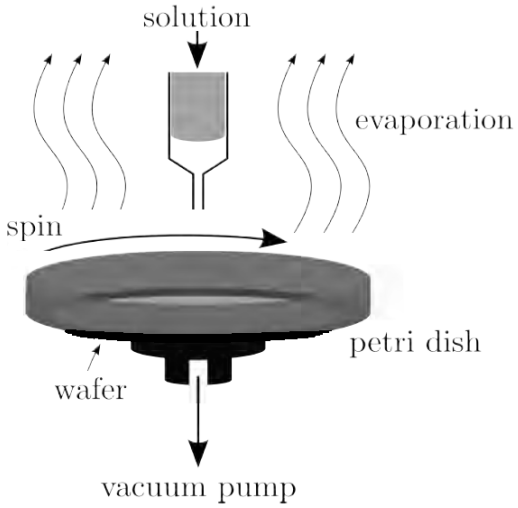

Figure 1. Scheme of the spin coater rotational device showing the syringe containing the precursor solution, the spin direction, the Petri dish located over the wafer support and the vacuum supply.

2.3. Characterization of the fillers and MMMs

The cross section of the prepared membranes was observed on an Inspect F *Scanning electron microscope (SEM)* to examine the membrane structure and evaluate the filler dispersion within the membrane and the filler-polymer contact. Previous freeze-fracturing of the membranes after immersion in liquid N_2 was required for this purpose.

Thermogravimetric analyses (TGA) were performed using a Mettler Toledo TGA/SDTA 851e instrument. Powder samples and MMMs (10 mg) placed in 70 µL alumina pans were heated in air flow from 25 ºC to 850 ºC at a rate of 10 ºC/min.

Differential scanning calorimetry (DSC) measurements were carried out using Mettler Toledo DSC822e equipment to estimate the glass transition temperature (T_g) of the MMMs containing the different fillers. Small pieces of dried membranes (10 mg) were transferred to 100 µL aluminum pans, which were hermetically sealed with aluminum covers. The samples were scanned from room temperature to 250 ºC with a

heating rate of 20 ºC/min. Two consecutive runs were performed for each sample and T_g was calculated from the inflection point of the slope transition in the DSC curve. The reported T_g values are the average based on the second run of 2-3 samples.

Mechanical strength measurements of the membranes were carried out under ambient conditions using a *dynamic mechanical analyzer (DMA)* (01 dB-Metravib) at a frequency of 2 Hz. Thin film strips with approximate dimensions (thickness x width x length) of ~0.03 x 5 x 15 mm^3 were clamped in the jaws. Then, pretension (static displacement of 75 μm) was applied for undulating tension operation (dynamic displacement of 25 μm). Young´s moduli were obtained from the stiffness and the geometry of the sample.

Contact angle (CA) was measured by means of a Dataphysics NEURTEK instrument. The angle was obtained from the upper surface of the membranes by depositing drops of distilled water (5 μL) with a microsyringe. At least 6 measurements in different areas of the films were taken to obtain the mean value.

X-ray diffraction (XRD) was applied to have a better understanding of the structure and crystallinity of the prepared fillers and MMMs using a D-Max Rigaku X-ray diffractometer (copper anode, graphite monochromator to select Cu-$K_{\alpha 1,2}$ radiation at λ = 1.5418 Å). Measurements were taken at room temperature from 2θ = 2.5º to 40º, step = 0.03º and t = 1s/step.

Fourier transform infrared spectroscopy (FTIR) of the membranes was performed on a Bruker Vertex 70 FTIR spectrometer equipped with a DTGS detector and a Golden Gate diamond ATR accessory. Powder samples were prepared by the KBr wafer technique and the measurements were done in a diffuse reflectance module. Both spectra were recorded by averaging 40 scans in the 4000-600 cm^{-1} wavenumber range at a resolution of 4 cm^{-1}. Data were registered with OPUS software from Bruker Optics.

Membrane thicknesses were tested by a Digimatic Micrometer (measurement range from 0 to 30 mm with an accuracy of ± 1 µm). A number of points (9) equally distributed on the membrane were measured per membrane and were used to achieve an arithmetic average for the membrane thickness. The standard deviation is later shown in Fig. 2 and Table 1. For permeation testing of the membranes, circular areas of 15.2 cm^2 were cut from the films.

2.4. Gas separation measurements of the MMMs

Permeability (*P*) of a gas and *Selectivity* ($\alpha_{i/j}$) (preferential permeating component *i* over component *j*) are the basic parameters governing membrane performance. *P* is defined as the permeance *Q* (pressure- and area-normalized flux, *N*, through the membrane) normalized by the thickness *l*, as Eq. 1 shows:

$$P = Q \cdot l = \frac{N \cdot l}{A \cdot \Delta p} \qquad \text{(Eq. 1)}$$

where *A* is the surface area of the membrane, and Δp is the partial pressure difference for separation. *P* is usually given in Barrer unit (Barrer = 10^{-10} $cm^3(STP) \cdot cm \cdot cm^{-2} \cdot s^{-1} \cdot cmHg^{-1}$). The ideal selectivity ($\alpha_{i/j}$) is the ratio of the pure gases: *i* and *j*, and is defined in Eq. 2:

$$\alpha_{i/j} = P_i / P_j = \frac{N_i \cdot (p_{feed,j} - p_{permeate,j})}{N_j \cdot (p_{feed,i} - p_{permeate,i})} \qquad \text{(Eq. 2)}$$

However, in gas mixtures both gases can affect each other in their permeation behaviour. The mixed-gas permeability is determined using Eq. 3:

$$P_i = \frac{N \cdot x_{permeate,i} \cdot l}{A \cdot (p_{feed} \cdot x_{feed,i} - p_{permeate} \cdot x_{permeate,i})} \qquad \text{(Eq. 3)}$$

where P_i is the mixed-gas permeability of gas *i*, and $x_{feed,i}$ and $x_{permeate,i}$ are the mole fractions of the gas *i*. Mixed-gas selectivity or separation factor expresses the relative

enrichment in the permeate stream with respect to the feed composition when a gas mixture is fed to the membrane system. It is calculated in Eq. 4:

$$\alpha_{i/j} = \frac{x_{permeate,i} \cdot (p_{feed} \cdot x_{feed,j} - p_{permeate} \cdot x_{permeate,j})}{x_{permeate,j} \cdot (p_{feed} \cdot x_{feed,i} - p_{permeate} \cdot x_{permeate,i})} \quad \text{(Eq. 4)}$$

being x_i and x_j, in mixed-gas selectivity the mole fractions of components *i* and *j* in the feed and permeate streams.

In this work, mixed-gas permeation tests were done. The membranes were introduced into the permeation module consisting of two stainless steel pieces and a macroporous disk support 316LSS with a 20 µm nominal pore size (Mott. Corp.) and gripped Viton® o-rings. The feed mixture (50/50 vol.% H_2/CH_4 or O_2/N_2) passed to the membrane by means of two (Alicat Scientific) mass-flow controllers (total flow of 50 cm^3(STP)/min) at 310-330 kPa. The permeate side of the membrane was swept with a 1 cm^3(STP)/min mass flow controlled stream of Ar for the H_2/CH_4 mixture, and 5 cm^3(STP)/min of He when separating the O_2/N_2 mixture, at 110-120 kPa, slightly higher than the atmospheric pressure. The outgoing gas concentrations were analyzed by an on-line gas micro-chromatograph (Agilent 3000A) equipped with a thermal conductivity detector (TCD). Measurements were performed at 35 ºC controlled by a UNE 200 oven (Memmert) and permeabilities were calculated once the exit gas flow had stabilized.

3. RESULTS AND DISCUSSION

3.1. Study of the spin coating parameters

The use of spin coating for ready-to-use membranes has several advantages over the traditional by-hand preparation method: (*i*) the thickness of the membrane is thin and tailorable, (*ii*) solvent evaporation is enhanced; and (*iii*) it constitutes an automatic (more mechanical) process. In this research, membranes were prepared by the

application of a certain amount of the membrane precursor solution on a rotating Petri dish. During the rotation process an outward force takes effect on the applied solution and the membrane is formed while the solvent evaporates. The spreading, the membrane formation and the properties of the final membrane are influenced by the interplay of the centrifugal driving force and the viscous resisting force of the fluid (Bornside et al., 1989).

As one of the main interests in the spin coater is its impact on the film thickness during and after the spin coating process, adjustable parameters such as the spinning disk velocity, rotational time and the viscosity of the solution were studied. Another factor was the amount of solution that is used, i.e., the initial height. It should be mentioned that in regular wafer coating the influence of the initial height can be ignored as long as sufficient solution is used (Schubert and Dunkel, 2003).

Fig. 2 shows the influence of these four parameters: (a) rotational speed, (b) precursor volume, (c) solid concentration, and (d) rotational time. First, in Fig. 2a the membrane thickness as a function of the *rotational speed* is presented. The velocity of the rotating Petri dish directly influenced the spreading of the membrane precursor on the dish and the evaporation of the solvent. The membrane thickness, from 55 to 25 μm, decreased as a function of the rotational velocities, from 250 to 650 rpm, when keeping the rest of the parameters constant (12.5 wt.% of solid in precursor, 3 mL of precursor volume, and 4 min of rotational time). Additionally, the standard deviation corresponding to the membrane thickness decreased with the rotational speed, leading to non-uniform membrane thicknesses at 250 rpm. Lower velocities were therefore not practical. Nevertheless, higher velocities led to a greater loss of applied precursor volume, as this spread to the outer regions of the Petri dish that were later cut out and discarded. At even higher velocities, from 650 rpm on, a spill out of the precursor

volume over the edge of the Petri dish occurred. It is worth noting that pure PSF films were used to study the rest of the parameters; however, in this case, a MMM based on ETS-10 (8 wt.% loading) in PSF matrix was used (Fig. 2a).

The second parameter to adjust is the amount of *precursor volume* used for the fabrication of each membrane. With less volume of solution, thinner membranes were expected. Fig. 2b shows the tendencies of bare PSF film thicknesses from the lower to the higher rotational velocities previously selected for two different membrane precursor volumes. At low rpm there was no difference in membrane thickness, but standard deviation was greater for a higher precursor volume. At medium velocities, the differences in membrane thickness between the 2 and 3 mL precursor volumes were about 10 μm for 350 rpm and 5 μm for 450 rpm. At higher velocities the excess precursor volume spread to the edge of the Petri dish. Comparing Fig. 2a with Fig. 2b, it can be seen that standard deviation was generally a little lower for pure PSF membranes than for the ETS-10 MMMs.

The *solid concentration*, i.e. the wt.% ((filler + polymer) / (filler + polymer + solvent)), and in the case of bare polymer membrane wt.% (polymer / (polymer + solvent)), was set during the preparation of the precursor solution. Higher viscosities would need greater spinning disk velocities to spread the membrane precursor solution because the higher polymer concentration, the higher the viscosity. Fig. 2c represents the thickness of PSF films prepared at two different solid concentrations: 12.5 and 15 wt.% PSF in the PSF-chloroform solution, setting the precursor volume at 3 mL and the rotation time at 2 min. A great influence of the PSF concentration on the membrane thickness can be observed at lower velocities. The standard deviation was greater at higher PSF concentrations at the lower velocities. Homogeneous membranes could be

prepared at lower PSF concentrations or at higher velocities, where the difference in membrane thicknesses decreased.

Finally, the *rotational time* of the spin coating process was varied in the second step of the two spin coating sequences, from 1 to 5 min, fixing the precursor solution volume at 2 mL, the PSF concentration at 12.5 wt % and the rotational speed at 450 rpm. As can be seen in Fig. 2d, the rotation duration did not show any clear influence on the membrane thickness, which ranged from 35 to 42 μm. Thus, the membrane thickness was basically set by the other parameters at an early stage of the rotation time.

As a result, with the aim of obtaining a thin but reproducible membrane, various pure PSF membranes and MMMs with a specific filler loading of 8 wt.% for each type of material were prepared using the same spin coating parameters and conditions. In general, medium-to-lower velocities where selected, inducing a reduction in stress on the forming membrane. This was first, to avoid the high-thickness standard deviation that occurred when using too low rpm, and second to avoid the loss of large amounts of precursor volume. For a good processability, i.e. to allow a sufficient rotational speed to spread the membrane material on the Petri dish in a homogeneous manner, the lower solid concentration of the precursor solution was selected, being low enough to control the solvent evaporation. The following parameters were chosen for the characterization test series: (a) 350 rpm rotational speed, (b) 2-3 mL precursor volume per membrane, (c) 12.5 wt.% solid concentration (polymer or polymer and filler), and (d) 1 min rotation duration.

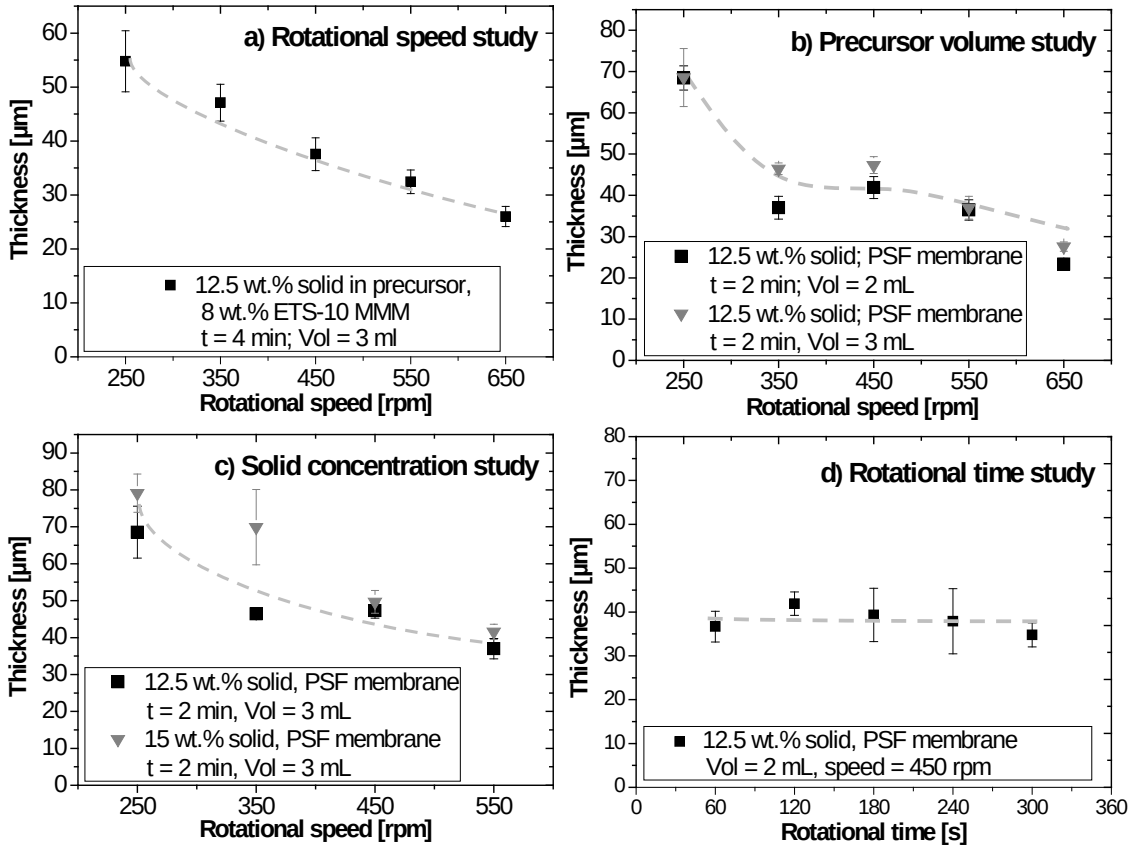

Figure 2: Parameter study of membranes prepared via spin coating: a) influence of the rotational speed for a MMM based on ETS-10 (8 wt.% loading), b) influence of the precursor volume for a PSF membrane, c) influence of the solid concentration for a PSF membrane, and d) influence of the rotational time for a PSF membrane.

It should be noted that in the fabrication of MMMs via spin coating the solvent evaporates fast and is released more quickly compared with the traditional casting method due to the rotation of the Petri dish support forming the membrane in a short period of time. The ETS-10, MCM-41 silica spheres and NH_2-MIL-53 fillers were distributed homogeneously within the polymer across the whole thickness of the membrane. Those prepared with ZIF-8 suffered some particle agglomeration (see Fig. S1). In general, sedimentation of the fillers was prevented with the proper selection of the rotational speed and time of the spin coater, and a homogeneously axial and radial

filler distribution in the PSF matrix was ensured. By this technique, MMMs with as little as 20 μm thickness were successfully prepared.

3.2.Characterization of MMMs prepared via spin coating

Cross-sectional SEM micrographs of MMMs comprising 8 wt.% loading of ETS-10, MCM-41, ZIF-8 and NH_2-MIL-53 are shown in Fig. 3. The ETS-10 particles have a size of 400-700 nm depending on the particle plane (Fig. 3a). Despite minor agglomerations, the particles are well dispersed in the polymer matrix showing good contact with the PSF. It should be considered that the apparent sieve-in-cage morphologies may well come from the SEM-preparation by freeze-fracturing after immersion in liquid N_2 (Zornoza et al., 2011a).

Fig. 3b shows silica spheres of around 400 nm diameter immersed in the polymer phase. The pore diameter of this MCM-41-type structure of around 2.8 nm allows the penetration of PSF chains into the mesopores, promoting the formation of an intimate contact between both phases (Zornoza et al., 2009). Also, the spherical shape limits the contact between particles giving good dispersion without interfacial gaps between the filler and the polymer.

MOFs have an evident advantage over zeolites or silica from the point of view of compatibility between the polymer phase and the filler. Due to their partially organic nature, MOF interaction with the polymer is favored. ZIF-8 and NH_2-MIL-53 MOFs (Fig. 3c-d) are dispersed inside the polymer matrix creating a certain degree of aggregation of individual particles of about 85 nm, relatively smaller in size than those of the ETS-10 and MCM-41.

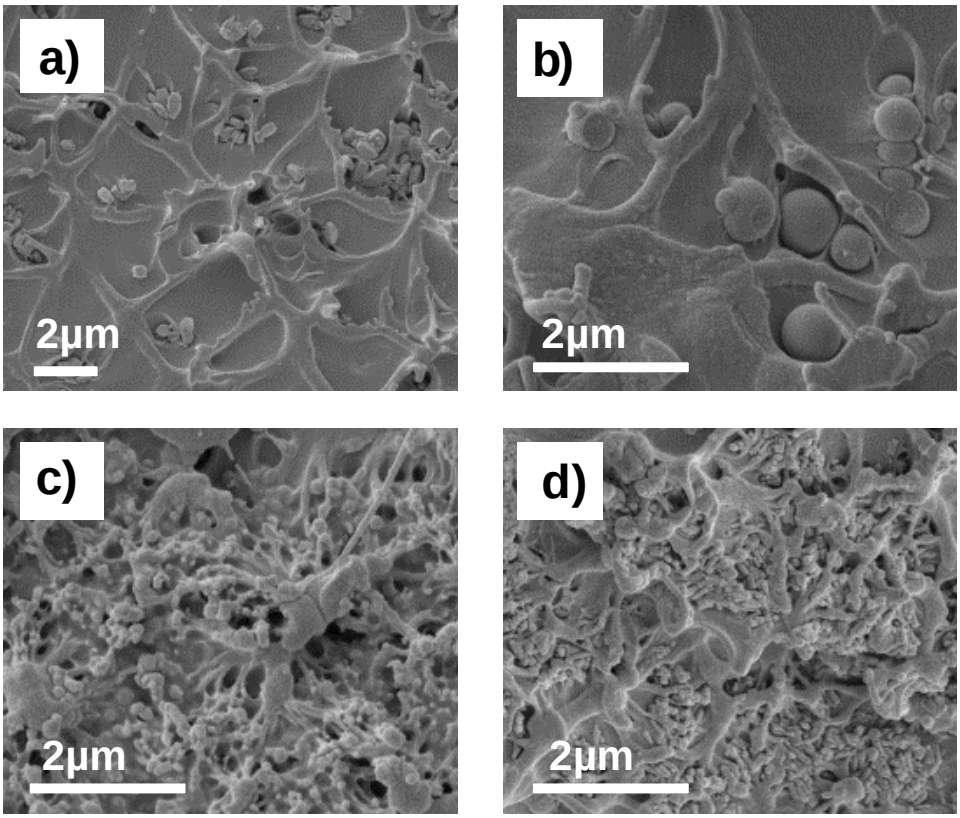

Figure 3. SEM images of the cross section of MMMs prepared with spin coating technology: a) 8 wt.% ETS-10 MMM, b) 8 wt.% MCM-41 silica spheres MMM, c) 8 wt.% ZIF-8 MMM, and d) 8 wt.% NH_2-MIL-53 MMM.

Some of the most important characterization parameters of the fillers and MMMs are depicted in Table 1. Apart from the nature, size, shape, and BET specific surface area and pore diameter of the particles, the T_g, Young's moduli and contact angle values of the MMMs were evaluated, these parameters being more directly related to the distribution and interaction of the filler within the polymer. In addition, the membrane thicknesses for each type of filler whose gas separation performance are plotted in Figs. 5-7 are given. Note the thickness difference obtained between the PSF membrane, MCM-41 MMM and NH_2-MIL-53 MMM of about 30 µm, and between the ETS-10 MMM and ZIF-8 MMM of about 50 µm, when manually spreading 2 or 3 mL of

precursor volume, respectively, from the syringe onto the rotating Petri dish. All these characterization parameters provide a better insight into the gas separation performance.

Table 1. Characterization features of fillers and MMMs prepared with ETS-10, silica spheres, ZIF-8 and NH_2-MIL-53.

	Filler				**8% filler-PSF MMM**				
	Nature	**Shape & size**	**Pore diameter (nm)**	**BET area (m^2/g)**	**TGA loading (wt.%)**	**T_g (ºC)**	**Young´s modulus (GPa) [a]**	**Contact angle (º) [b]**	**Film thickness [µm] [c]**
Polysulfone (PSF)	amorphous polymer	-	-	-	-	188.5	1.87 (±0.14)	81.6 (±2.3)	32.6 (±5.0)
ETS-10	Inorganic: porous titanosilicate	Square truncated bipyramid 400-700 nm	0.49x0.76	253 (Casado et al., 2009)	8.2	189.2	(-)	86.1 (±3.4)	46.2 (±1.6)
MCM-41	Inorganic: mesoporous ordered material	Spherical ~ 400 nm	2.8	1100 (Grün et al., 1997)	8.4	189.6	2.09 (±0.11)	84.3 (±2.5)	26.5 (±3.5)
ZIF-8	Metal-organic material	Polyhedron ~85 nm	0.34	1079 (Pan et al., 2011)	8.5	188.9	1.31 (±0.14)	(-)	52. 9 (±6.1)
NH_2-MIL-53	Metal-organic material	Rounded < 100 nm	0.75	675 (Gascon et al., 2009)	8.0	189.0	1.57 (±0.12)	85.9 (±2.5)	27.0 (±2.6)

[a] Standard deviation refers to the error in the measurement of the membrane.

[b] Standard deviation refers to 6 different points tested in the same membrane.

[c] Standard deviation refers to 9 different points measured in the same membrane. Membranes of bare PSF, MCM-41 and NH_2-MIL-53 were prepared with 2 mL of precursor volume while membranes of ETS-10 and ZIF-8 were prepared with 3 mL of precursor volume.

(-) Not tested in this work.

Thermogravimetric analyses of the fillers (Fig. S2) and MMMs with 8 wt.% nominal loading (Fig. S3) were performed to verify the amount of filler in the prepared MMMs and to check the thermal stability of the MMMs. The account of total accumulated weight loss gave the nominal loading of inorganic filler present in the corresponding MMM, i.e. 8.2 wt.% ETS-10 and 8.4 wt.% MCM-41. In the case of the MOFs, the material remaining after 700 ºC was attributed to the corresponding metal oxide phase. Thus, giving the amount of organic linker allows one to obtain the MOF loading within the MMM, i.e. 8.5 wt.% ZIF-8 and 8.0 wt.% NH_2-MIL-53. It can be seen that with the embedding of MOF fillers, the decomposition of the fillers is shifted to higher temperatures which may be due to the transport limitations generated by the surrounding polymer.

T_g values and dynamical mechanical analyses of the MMMs were also compared in Table 1, giving information about the rigidity of the membrane, the flexibility of the polymer chains and the interaction strength. In contradiction with the expected behavior of restricted motion of the polymer due to the chemical interactions between the polymer chains and the filler external surface area, only a slight increase in T_g with respect to the PSF membrane was obtained, coming close to experimental error. This suggests that there is no substantial influence of the filler on the polymer matrix towards higher rigidity, as previously observed for MOF-containing MMMs (Basu et al., 2011; Diaz et al., 2011). The greater mobility of the MOF fillers with their organic groups leads to a less strong stiffening and lesser influence on the thermal properties of the MMM than the ETS-10 titanosilicate or the MCM-41 silica spheres. On the other hand, in the case of the inorganic filler, there was an increase in T_g (5 ºC) when incorporating 8 wt.% mesoporous silica spheres of about 3 µm size into the PSF MMMs prepared by the traditional casting method (Zornoza et al., 2011a).

With the addition of inorganic filler, the Young's modulus of the pure polymer thin film increased from 1.87 to 2.09 GPa for the MCM-41-MMMs, while the parameter decreased for the MOF-MMMs. The stiffening effect of the rigid silica particles caused the MMMs to become harder. However, a decrease in rigidity when embedding MOFs within the polymer phase was visible. This could be explained by their flexible structure. In fact, when incorporating a drug model (i.e. caffeine) into ZIF-8, even though the MOF has small pore apertures of 3.4 Å, its flexible structure permits a 28 wt.% loading of guest encapsulated molecules with molecular size exceeding by far the pore aperture dimension (Liedana et al., 2012). In addition, the mechanical stability can be altered due to the greater stress induced from the solvent evaporation during the membrane preparation by spin coating compared with by-hand casting. This stress could increase because of the faster solvent evaporation via spin coating. To complement this study, Table 1 also lists the results of the contact angle measurements. Despite the hydrophilic nature of the fillers with surface OH-groups (MCM-41, ETS-10 and NH_2-MIL-53), overall hydrophobicity was found that exceeded even the hydrophobicity of the pure polymer.

X-ray diffraction was used to study the arrangement of the fillers and the structural changes of the polymer chains of the plain PSF membranes and the MMMs, and to verify that the structure of the fillers was not altered once embedded in the PSF matrix. As Fig. 4 shows, the inter-chain spacing of 0.51 nm ($2\theta = 17.6^{\circ}$) of the PSF is slightly reduced for the MMMs ($2\theta = 17.8^{\circ}$). This implies a little tightening of the polymer chains due to their close integration with the fillers, according to the SEM micrographs. Fillers within MMMs change their crystalline intensity and some peak displacements with respect to the filler materials are visible. Their structure may be deformed due to the polymer-filler interaction, and the shift strength basically depends on the nature and

pore structure of the filler. In general, deflection peaks for all the fillers shift to greater angles. In the case of ETS-10, displacements from 2θ = 25.8º to 26.0º, 27.2º to 27.3º, and 6.0º to 6.2º are visible. For MCM-41, the penetration of the PSF chains into the mesoporous channels of the silica may mitigate the disruption of the chain packing (Zornoza et al., 2009). The high surface MOFs induce the best contact of the tested fillers as the polymer chains were substantially altered to even greater angles. For ZIF-8, peak movements were found from 2θ = 7.3º to 7.6º, 10.3º to 10.7º, and 12.6º to 13.1º, and for NH_2-MIL-53, from 2θ = 9.0º to 9.1º, 10.0º to 10.2º and 18.2º to 18.3º. Unlike NH_2-MIL-53 synthesized with H_2O as solvent, when using DMF, a higher intensity of the first peak (2θ = 9.0º) is observed, characteristic of the MOF in its large pore (*lp*) form (Couck et al., 2009). In addition, at 11.9 º, the more indicative peak of the MOF in its narrow pore (*np*) structure is not marked within the MMM XRD pattern. In general, no major influence of the preparation method on the polymer-filler contact has been found, but the spin coating technology may intensify stresses inside the forming membrane due to the faster solvent evaporation.

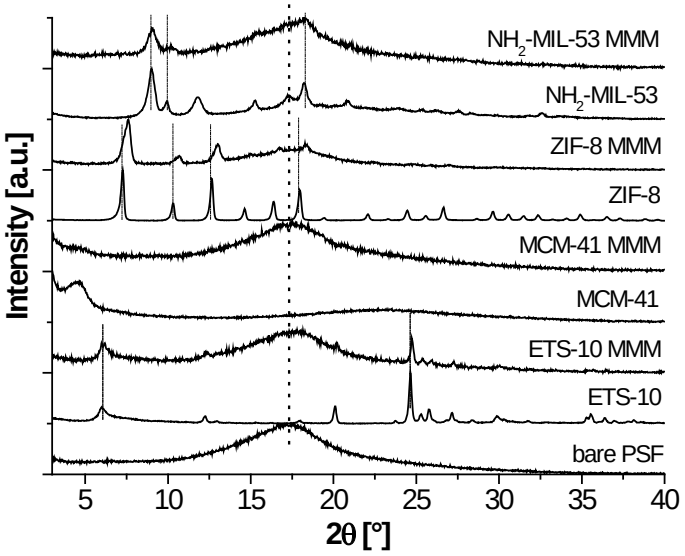

Figure 4. X-ray diffraction patterns of the different fillers and MMMs containing 8 wt.% of ETS-10, MCM-41, ZIF-8, NH_2-MIL-53, and pure PSF.

FTIR spectra of the bare polymer PSF and the 8 wt.% MMMs prepared with the two different inorganic and metal-organic fillers are shown in Fig. S4. The characteristic absorption peaks of ETS-10, MCM-41 silica spheres, ZIF-8, NH_2-MIL-53 and polymer are present in the spectra. The pure polymer peaks in the 900-1100 cm^{-1} region are assigned to C-C stretching, at 1150 and 1327 cm^{-1} to Ar-SO_2-Ar symmetric and asymmetric stretching, respectively, at 1235 cm^{-1} to Ar-O-Ar stretching vibration and at 1295 cm^{-1} to S=O stretching. It can be deduced that no strong chemical interactions between the polymer and filler are evident, or simply that not enough filler was added to the polymer to obtain such peak displacements. Small and increasing shifts to higher wavenumbers were found deriving from the aryl ether (Ar-O-Ar) vibrations of PSF interacting with the filler surface of mesoporous silica at higher loadings (Zornoza et al., 2009).

3.3. Gas permeation results

When using spin coating for membrane casting, the solvent evaporation during the process should be considered even if the rotational time has no influence on the membrane thickness. As stated above, this evaporation effect could generate a possible stress inside the membrane. This would result in the production of more defective and less stable membranes when compared with the controlled release of solvent in the by-hand casting process in which membranes are immediately capped after the solution is spread. It is worth mentioning that a general lower selectivity and slight increase in permeability were achieved for PSF membranes prepared by spin coating technology compared to those made by-hand (Zornoza et al., 2011a). For a fair comparison only the PSF-MMMs comprising ETS-10, MCM-41, ZIF-8 and NH_2-MIL-53 prepared in this work via spin coating were analyzed.

Mixed-gas separation results for the PSF and MMMs containing 8 wt.% of ETS-10, MCM-41 spheres, ZIF-8 and NH_2-MIL-53 are plotted in Fig. 5 (H_2/CH_4) and Fig. 6 (O_2/N_2), while Tables S1 and S2 detail the corresponding permeabilities and selectivity values. These tables show the results in both Barrer and GPU units. In these structurally engineered hybrid membranes, the fillers (porous silicates or MOFs) were applied with the purpose of creating preferential permeation pathways through their meso- or microporous structures to provide superior permeation properties. The separation performance of the MMMs varies greatly from the different capacity of the fillers to discriminate between the molecules present in the feed mixture.

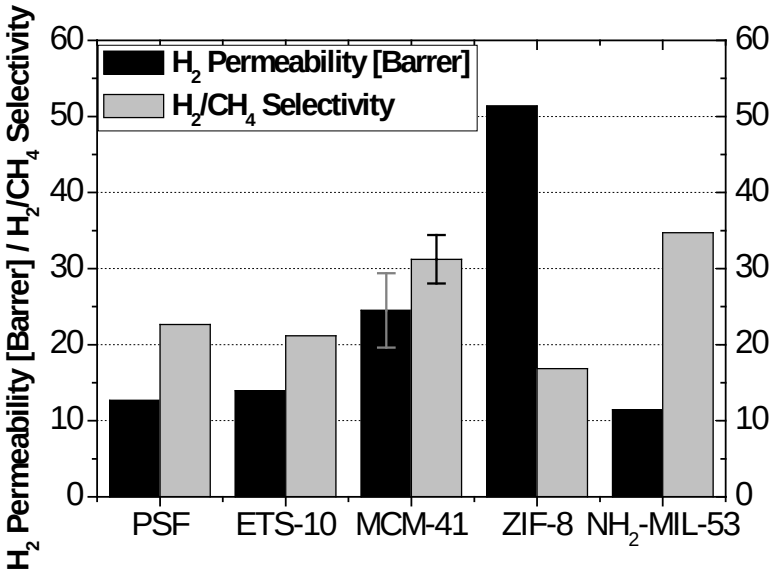

Figure 5. H_2 permeability and H_2/CH_4 selectivity for PSF and MMMs comprising 8 wt.% of ETS-10, MCM-41, ZIF-8 and NH_2-MIL-53. Standard deviation of four different MCM-41 MMMs is also given.

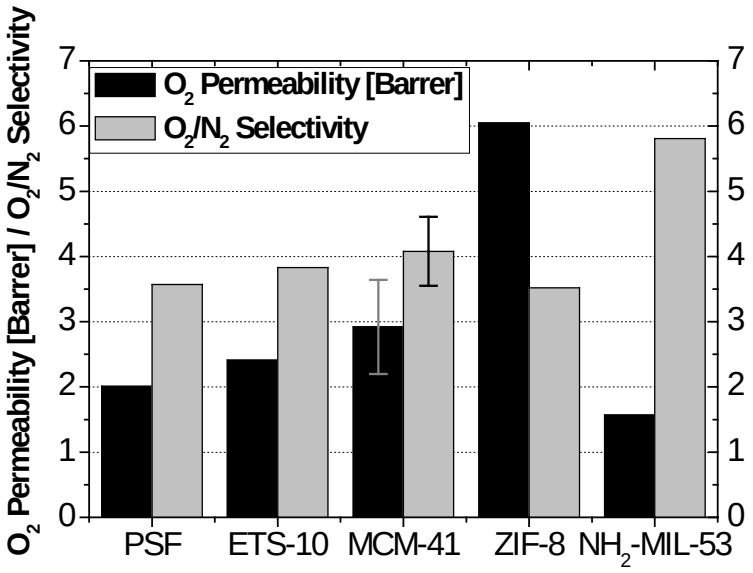

Figure 6. O_2 permeability and O_2/N_2 selectivity for PSF and MMMs comprising 8 wt.% of ETS-10, MCM-41, ZIF-8 and NH_2-MIL-53. Standard deviation of four different MCM.41 MMMs is also given.

The MMMs based on the titanosilicate ETS-10 showed no significant to no-improvement in gas permeability/selectivity compared to the bare polymer film. However, the MMMs comprising MCM-41 silica spheres of about 400 nm in diameter size achieved both superior permeability and selectivity for the H_2/CH_4 and O_2/N_2 gas mixtures. The same trend of increasing permeability and selectivity values had previously been observed in mesoporous silica spheres (MSSs) -PSF or -Matrimid® MMMs, also for 8 wt.% loading, for H_2/CH_4 and CO_2/N_2 separations (Zornoza et al., 2011a). In the case of the MCM-41 MMM, the polymer chains were able to penetrate into the mesoporosity of the filler, favoring gas diffusivity. The reactive silanol groups helped bringing the polymer chain through hydrogen bonding. As regards the spherical shape of these materials, which limits the contact among them, a good distribution without appreciable agglomeration was observed (Fig. 3b). In addition, the MMMs based on MCM-41 silica spheres turned out to be the most robust, as shown in Table 1,

with the highest T_g and Young´s modulus values. It should be noted that the permeation results for these membranes were calculated from four different samples, assuming the standard deviation to be in the same range as for the other MMMs.

The MOF MMMs led to the greatest selectivity using the NH_2-MIL-53 filler for both H_2/CH_4 and O_2/N_2 (34.7 with PH_2 = 11.5 Barrer, and 5.8 with PO_2 = 1.6 Barrer, respectively) and the greatest permeability when embedding ZIF-8 (PH_2 = 51.4 Barrer with $\alpha(H_2/CH_4)$ = 16.8 and PO_2 = 6.5 Barrer with $\alpha(O_2/N_2)$ = 3.5) of all the membranes tested. Intermediate permeability and selectivity values for O_2/N_2 were found in the literature for 8 wt.% MIL-101 (Cr) PSF MMM (PO_2 = 2.5 Barrer with $\alpha(O_2/N_2)$ = 5.3) Jeazet et al., 2012. MOF particles, both nanosized ZIF-8 and NH_2-MIL-53, have a similar particle size but smaller compared to the particle size of the silica spheres. This may have an influence on their polymer-filler interaction as some agglomeration of the MOF particles occurred (Fig. 3c-d). As regards the surface chemistry, in both metal-organic materials, the organic linkers that build their frameworks are more compatible with the polymer matrix. Besides, NH_2-MIL-53 has the additional advantage of pore flexibility upon adsorption of guest molecules, such as CO_2, H_2O and most organic solvents, changing reversibly their pore framework as well as the NH_2-group that strengthens the interaction with the polymer (Zornoza et al., 2011c).

Showing the data in vectorial form, the trade-off between membrane selectivity and permeability is more visible. Fig. 7 presents the selectivity (H_2/CH_4 or O_2/N_2) versus the permeability (H_2 or O_2) for the prepared MMMs, taking the pure PSF as the starting point of the arrow direction.

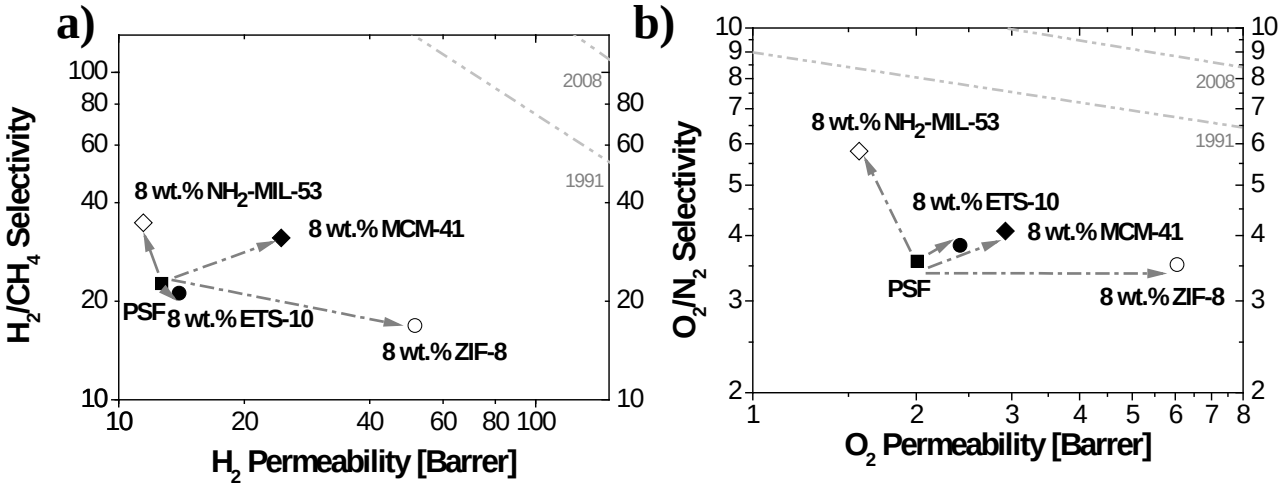

Figure 7. Permeability and selectivity for different MMMs for: a) H_2/CH_4 mixture and b) O_2/N_2 mixture, represented as vectorial distance from the pure PSF membrane.

The gas separation behavior of the MMMs containing the different fillers, as plotted in Fig. 7, could to a certain extent be related to the study of membrane defects among the filler-polymer phases detailed by Moore and Koros, 2005. These authors studied five cases of adverse morphologies and their effect on the membrane transport properties: (*i*) "rigidified polymer matrix layer",(*ii*) "sieve-in-a-cage morphology", (*iii*) "leaky interface", (*iv*) "clogged filler", and (*v*) "bottlenecked filler". For all MMMs the polymer chains could undergo some rigidification in the area surrounding the flexible fillers, although no significant changes in the T_g value have previously been. NH_2-MIL-53 MMMs, to some extent, could follow case (*i*), what establishes that the stress on the polymer chains during solvent evaporation induces a reduction in the free volume near the particle surface, thus obtaining lower permeabilities with an increase in selectivity. In contrast, the ZIF-8 MMM is more like case (*ii*), with a low selective and high free volume phase accounting for the agglomeration observed in Fig.3a. It is clear that the MCM-41 MMM performance came between that of the MOF MMMs, more pronounced for the H_2/CH_4 separation.

4. CONCLUSIONS

Uniformly symmetric dense mixed matrix membranes were successfully prepared by spin coating resulting in a feasible, reproducible and more automated membrane fabrication procedure compared to the classical by-hand casting method. An exhaustive study of the parameters affecting membrane formation by spin coating confirmed the possibility to tailor the membrane properties, selecting the appropriate rotational speed of the wafer support (350 rpm), precursor volume spread per membrane (2-3 mL), solid concentration (12.5 wt.%) and rotational time (1 min). Using these parameter values, this methodology of preparing MMMs at 8 wt.% loading was extended to four different porous fillers: inorganic (ETS-10 and MCM-41) and metal-organic (ZIF-8 and NH_2-MIL-53), with different particle sizes and shapes, and different pore structures.

Good interaction between the filler-polymer phases was confirmed by the characterization carried out by SEM, TGA, DSC, DMA, CA, XRD and FTIR. Choosing the appropriate filler, an enhancement in the performance of the MMMs for the separation of H_2/CH_4 and O_2/N_2 mixtures can be achieved when compared to the bare polymer membrane. Overall, the best results were obtained by using MCM-41 silica spheres or NH_2-MIL-53 particles as fillers. While the MCM-41 resulted in increased permeability and selectivity the strong selectivity of the NH_2-MIL-53 MMM came from the reduced permeability of the slow diffusing gas component (CH_4 or N_2). Besides, the use of ZIF-8 as filler resulted in a considerably increased permeability in the hybrid membrane compared to the neat PSF membrane, with a selectivity penalty for the H_2/CH_4 gas mixture.

Acknowledgments

The authors gratefully acknowledge the Spanish Ministry of Economy and Competitiveness (project MAT2010-15870) as well as the Regional Government of Aragón and the European Social Fund.

REFERENCES

Ahn, J., Chung, W.-J., Pinnau, I., Guiver, M. D., 2008. Polysulfone/silica nanoparticle mixed-matrix membrane for gas separation. J. Membr. Sci. 314, 123.

Aroon, M. A., Ismail, A. F., Matsuura, T., Montazer-Rahmati, M. M., 2010. Performance studies of mixed matrix membranes for gas separation: A review. Sep. Purification Technol. 75, 229.

Bae, T. H., Lee, J. S., Qiu, W., Koros, W. J., Jones, C. W., Nair, S., 2010. A high-performance gas-separation membrane containing submicrometer-sized metal-organic framework crystals. Angew. Chem. Int. Ed. 49, 9863.

Basu, S., Cano-Odena, A., Vankelecom, I. F. J., 2011. MOF-containing mixed-matrix membranes for CO(2)/CH(4) and CO(2)/N(2) binary gas mixture separations. Sep. Purification Technol. 81, 31.

Bernardo, P., Drioli, E., Golemme, G., 2009. Membrane Gas Separation: A Review/State of the Art. Ind. Eng. Chem. Res. 48, 4638.

Bornside, D. E., Macosko, C. W., Scriven, L. E., 1989. Spin coating - one dimensional model. J. Appl. Phys. 66, 5185.

Casado, C., Amghouz, Z., Garcia, J. R., Boulahya, K., Gonzalez-Calbet, J. M., Tellez, C., Coronas, J., 2009. Synthesis and characterization of microporous titanosilicate ETS-10 obtained with different Ti sources. Materials Research Bulletin 44, 1225.

Couck, S., Denayer, J. F. M., Baron, G. V., Remy, T., Gascon, J., Kapteijn, F., 2009. An amine-functionalized MIL-53 metal-organic framework with large separation power for CO_2 and CH_4. J. Am. Chem. Soc. 131, 6326.

Cui, L. L., Qiu, W. L., Paul, D. R., Koros, W. J., 2011. Responses of 6FDA-based polyimide thin membranes to CO2 exposure and physical aging as monitored by gas permeability. Polymer 52, 5528.

Chung, T. S., Jiang, L. Y., Li, Y., Kulprathipanja, S., 2007. Mixed matrix membranes (MMMs) comprising organic polymers with dispersed inorganic fillers for gas separation. Prog. Polym. Sci. 32, 483.

Diaz, K., Lopez-Gonzalez, M., del Castillo, L. F., Riande, E., 2011. Effect of zeolitic imidazolate frameworks on the gas transport performance of ZIF8-poly(1,4-phenylene ether-ether-sulfone) hybrid membranes. J. Membr. Sci. 383, 206.

Gascon, J., Aktay, U., Hernandez-Alonso, M. D., van Klink, G. P. M., Kapteijn, F., 2009. Amino-based metal-organic frameworks as stable, highly active basic catalysts. J. Catal. 261, 75.

Goh, P. S., Ismail, A. F., Sanip, S. M., Ng, B. C., Aziz, M., 2011. Recent advances of inorganic fillers in mixed matrix membrane for gas separation. Sep. Purification Technol. 81, 243.

Grün, M., Lauer, I., Unger, K. K., 1997. The synthesis of micrometer- and submicrometer-size spheres of ordered mesoporous oxide MCM-41. Adv. Mater. 9, 254.

Husain, S., Koros, W. J., 2007. Mixed matrix hollow fiber membranes made with modified HSSZ-13 zeolite in polyetherimide polymer matrix for gas separation. J. Membr. Sci. 288, 195.

Itta, A. K., Tseng, H. H., Wey, M. Y., 2010. Effect of dry/wet-phase inversion method on fabricating polyetherimide-derived CMS membrane for H-2/N-2 separation. International Journal of Hydrogen Energy 35, 1650.

Itta, A. K., Tseng, H. H., Wey, M. Y., 2011. Fabrication and characterization of PPO/PVP blend carbon molecular sieve membranes for H-2/N-2 and H-2/CH4 separation. J. Membr. Sci. 372, 387.

Jeazet, H. B. T., Staudt, C., Janiak, C., 2012. A method for increasing permeability in O-2/N-2 separation with mixed-matrix membranes made of water-stable MIL-101 and polysulfone. Chem. Commun. 48, 2140.

Jiang, L. Y., Chung, T. S., Kulprathipanja, S., 2006. Fabrication of mixed matrix hollow fibers with intimate polymer-zeolite interface for gas separation. AIChE J. 52, 2898.

Kim, S., Chen, L., Johnson, J. K., Marand, E., 2007. Polysulfone and functionalized carbon nanotube mixed matrix membranes for gas separation: Theory and experiment. J. Membr. Sci. 294, 147.

Kulprathipanja, S., Neuzil, R. W., Li, N. N.; to AlliedSignal, Inc., USA.: 1988.

Leroux, J. D., Paul, D. R., 1992. Preparation of composite membranes by a spin coating process. J. Membr. Sci. 74, 233.

Li, Y., Chung, T. S., Huang, Z., Kulprathipanja, S., 2006. Dual-layer polyethersulfone (PES)/BTDA-TDI/MDI co-polyimide (P84) hollow fiber membranes with a submicron PES-zeolite beta mixed matrix dense-selective layer for gas separation. J. Membr. Sci. 277, 28.

Liedana, N., Galve, A., Rubio, C., Tellez, C., Coronas, J., 2012. CAF@ZIF-8: One-Step Encapsulation of Caffeine in MOF. Acs Applied Materials & Interfaces 4, 5016.

Merkel, T. C., Freeman, B. D., Spontak, R. J., He, Z., Pinnau, I., Meakin, P., Hill, A. J., 2002. Ultrapermeable, reversible-selective nanocomposite membranes. Science 296, 519.

Moore, T. T., Koros, W. J., 2005. Non-ideal effects in organic-inorganic materials for gas separation membranes. J. Mol. Struct. 739, 87.

Moore, T. T., Damle, S., Williams, P. J., Koros, W. J., 2004. Characterization of low permeability gas separation membranes and barrier materials; design and operation considerations. J. Membr. Sci. 245, 227.

Oztekin, A., Bornside, D. E., Brown, R. A., Seidel, P. K., 1995. The connection between hydrodynamic stability of gas flow in spin coating and coated film uniformity. J. Appl. Phys. 77, 2297.

Pan, Y. C., Liu, Y. Y., Zeng, G. F., Zhao, L., Lai, Z. P., 2011. Rapid synthesis of zeolitic imidazolate framework-8 (ZIF-8) nanocrystals in an aqueous system. Chem. Commun. 47, 2071.

Rafizah, W. A. W., Ismail, A. F., 2008. Effect of carbon molecular sieve sizing with poly(vinyl pyrrolidone) K-15 on carbon molecular sieve-polysulfone mixed matrix membrane. J. Membr. Sci. 307, 53.

Rao, P. S., Wey, M. Y., Tseng, H. H., Kumar, I. A., Weng, T. H., 2008. A comparison of carbon/nanotube molecular sieve membranes with polymer blend carbon molecular sieve membranes for the gas permeation application. Microporous Mesoporous Mater. 113, 499.

Reid, B. D., Ruiz-Trevino, A., Musselman, I. H., Balkus, K. J., Ferraris, J. P., 2001. Gas permeability properties of polysulfone membranes containing the mesoporous molecular sieve MCM-41. Chem. Mater. 13, 2366.

Robeson, L. M., 1991. Correlation of separation factor versus permeability for polymeric membranes. J. Membr. Sci. 62, 165.

Robeson, L. M., 2008. The upper bound revisited. J. Membr. Sci. 320, 390.

Rubio, C., Casado, C., Gorgojo, P., Etayo, F., Uriel, S., Téllez, C., Coronas, J., 2010. Exfoliated titanosilicate material UZAR-S1 obtained from JDF-L1. Eur. J. Inorg. Chem., 159.

Schubert, D. W., Dunkel, T., 2003. Spin coating from a molecular point of view: its concentration regimes, influence of molar mass and distribution. Mater. Res. Innov. 7, 314.

Shen, Y., Lua, A. C., 2010. Effects of Membrane Thickness and Heat Treatment on the Gas Transport Properties of Membranes Based on P84 Polyimide. J. Appl. Polym. Sci. 116, 2906.

Tanh Jeazet, H. B., Staudt, C., Janiak, C., 2012. Metal-organic frameworks in mixed-matrix membranes for gas separation. Dalton transactions 41, 14003.

Tseng, H. H., Kumar, I. A., Weng, T. H., Lu, C. Y., Wey, M. Y., 2009. Preparation and characterization of carbon molecular sieve membranes for gas separation-the effect of incorporated multi-wall carbon nanotubes. Desalination 240, 40.

Vu, D. Q., Koros, W. J., Miller, S. J., 2003. Mixed matrix membranes using carbon molecular sieves: I. Preparation and experimental results. J. Membr. Sci. 211, 311.

Weng, T. H., Tseng, H. H., Wey, M. Y., 2010. Fabrication and characterization of poly(phenylene oxide)/SBA-15/carbon molecule sieve multilayer mixed matrix membrane for gas separation. International Journal of Hydrogen Energy 35, 6971.

Zhang, X., Lu, H. J., Soutar, A. M., Zeng, X. T., 2004. Thick UV-patternable hybrid sol-gel films prepared by spin coating. J. Mater. Chem. 14, 357.

Zimmerman, C. M., Mahajan, R., Koros, W. J., 1997. Fundamental and practical aspects of mixed matrix gas separation membranes. Abstr. Paper. Am. Chem. Society 214, 270.

Zornoza, B., Tellez, C., Coronas, J., 2011a. Mixed matrix membranes comprising glassy polymers and dispersed mesoporous silica spheres for gas separation. J. Membr. Sci. 368, 100.

Zornoza, B., Irusta, S., Tellez, C., Coronas, J., 2009. Mesoporous silica sphere-polysulfone mixed matrix membranes for gas separation. Langmuir 25, 5903.

Zornoza, B., Esekhile, O., Koros, W. J., Tellez, C., Coronas, J., 2011b. Hollow silicalite-1 sphere-polymer mixed matrix membranes for gas separation. Sep. Purification Technol. 77, 137.

Zornoza, B., Martinez-Joaristi, A., Serra-Crespo, P., Tellez, C., Coronas, J., Gascon, J., Kapteijn, F., 2011c. Functionalized flexible MOFs as fillers in mixed matrix membranes for highly selective separation of CO(2) from CH(4) at elevated pressures. Chem. Commun. 47, 9522.